DOI: 10.24996/ijs.2026.67.7.36

ISSN: 0067-2904

Numerical Simulation of a Multilayer Perceptron Neural Network for Predicting and Correcting the Wavefront in an Adaptive Optics System for Closed and Open Loops

Hayder Hasan Jawad*, Raaid Nawfee Hassan
Department of Astronomy and Space, College of Science, University of Baghdad, Baghdad, Iraq

Received: 7 /11/2024 Accepted: 21/7/2025 Published: 30/ 7/2026

Abstract

This paper presents a numerical simulation of a multilayer perceptron neural network (MLPNN) for predicting and correcting the disturbed wavefront in both closed and open loops in adaptive optics systems. Traditional adaptive optics systems often encounter limitations restraining their efficiency. The MLPNN model was implemented to reduce the challenges by enhancing prediction and correction accuracy in both closed and open loops. It was trained and tested over a wide range of turbulence marked by Fried parameters (r_0) . Under weak turbulence, $(r_0 = 0.2m)$ closed loop achieved a Strehl ratio (SR) up to 0.9283 and the average RMSE (ARMSE) of 0.2857 compared to 0.8414 for SR and 0.4411 ARMSE for open loop. In strong turbulence, $(r_0 = 0.08m)$ SR was 0.4328 and 0.9394 for ARMSE in closed loop, whilst SR degraded to 0.1467 with a rise in ARMSE to 1.3732 in open loop. Compared to the traditional method, SR improved by up to 38% and reduced ARMSE by up to 99%. These results confirm that closed loop consistently outperformed in both high and low turbulence conditions using the MLPNN approach.

Keywords: Adaptive Optics, Closed loop system, MLPNN, Open loop system, Optical Turbulence, and Strehl ratio.

محاكاة عددية لشبكة عصبية إدراكية متعددة الطبقات للتنبؤ وتصحيح جبهة الموجة لنظام البصريات التكيفية للدورات المغلقة والمفتوحة

حيدر حسن جواد* , رائد نوفي حسان
قسم الفضاء والفلك، كلية العلوم، جامعة بغداد، بغداد، العراق

الخلاصة

يقدم البحث نمذجة عددية للشبكة العصبية لبيرسبترون متعدد الطبقات (MLPNN) لغرض التنبؤ وتصحيح جبهة الموجه المشوهة في الدورات المغلقة والمفتوحة لمنظومة البصريات التكيفية حيث تواجه البصريات التكيفية التقليدية قيودا تحد من كفاءتها. وظف نموذج MLPNN للحد من التحديات عن طريق تحسين التنبؤ ودقة التصحيح في كل من الدورتين المغلقة والمفتوحة حيث درب واختبر لمدى واسع من

*Email: haidar.hasan2307@sc.uobaghdad.edu.iq

ظروف الاضطراب والمتمثلة بمعامل فريد (r_0). حققت الدورة المغلقة عند الاضطراب الواطئ $(r_0 = 0.2m)$ نسبة ستراها (SR) وصلت الى 0.9283 و0.2857 لمعدل جذر متوسط الخطأ (ARMSE) بالمقارنة مع SR البالغة 0.8414 و 0.4411 لARMSE في الدورة المفتوحة . تحت تأثير الاضطراب الشديد $(r_0 = 0.08m)$ حافظت الدورة المغلقة على SR قوية تبلغ 0.4328 و ARMSE بلغت 0.9394 على النقيض من الدورة المفتوحة التي انحدرت فيها SR الى 0.1467 وارتفعت ARMSE الى 1.3732 . تحسنت SR بنسبة 38% وانخفضت ARMSE بنسبة تصل الى 99% بالمقارنة مع الطريقة التقليدية. اثبتت النتائج ان معالجة الحلقة المغلقة ل MLPNN هي المثلى عند ظروف الاضطراب العالية والواطئة.

1. Introduction

The astronomical image observation of ground-based telescopes suffered from blurriness due to atmospheric fluctuations; therefore, the adaptive optics (AO) system was introduced as an elementary device to reduce aberration and enhance astronomical images [1]. It is known that the classic adaptive optics system detects the wavefront distorted shape with a wavefront sensor (WFS), then, the reconstruction process is executed by a deformable mirror (DM), where the control system manages this mechanism according to a specific algorithm [2]. The significant limitation of AO performance is time delay, which is the restricted time required between detection and correction. The disturbed wavefront considers the time-varying behaviour of atmospheric turbulence parameters [3]. Mainly, the ground-based telescopes of more than 1m apertures used for imaging with high resolution are supplied with an AO system [4]. The AO system control includes closed and open-loop control. The first one was mainly used in traditional AO systems in which the wavefront correction was highly accurate, but the limitation of system bandwidth restricted performance speed [5]. The open loop was implemented to provide a system bandwidth at the expense of remarkable accuracy [6]. The challenges of the AO system were due to the limitations represented by the time delay and the correction accuracy demanded by inserting the artificial neural network to overcome obstacles [3]. The artificial neural network represented by the multilayer perceptron neural network (MLPNN) was introduced to predict wavefront distortions due to atmospheric turbulence nonlinearity patterns to offset delays in the AO control system [7]. The training of MLPNN was implemented using the primary data from the wavefront sensor as inputs and the reconstructed phase aberration of the telescope as output, which enhanced the AO system [8].

MLPNN was implemented on an open-loop model with multi-object adaptive optics tomographic techniques. The atmospheric turbulence was high in simulated and accurate on-sky data [8-10]. Meanwhile, the Von Karman atmospheric turbulence model was employed in the MLPNN to compensate for phase distortion in the adaptive optics [11].
Despite the MLPNNs results focusing on open-loop AO systems, closed-loop AO applications are still underexplored, especially in the context of astronomical AO. Moreover, the dominance of model adaptive optics in wavefront correction, whereas the zonal correction, though it displays an extra direct and potentially accurate wavefront correction method, has limitations in neural network approaches. This makes a serious gap in our knowledge of MLPNNs in closed-loop, zonal-based AO systems, for the theoretical and practical partitions.

One of the research motivations is the rare employment of closed-loop neural networks, especially in astronomical adaptive optics, and the limited use of zonal model adaptive optics in wavefront correction, in exchange for focusing on the open loop system and model adaptive optics in wavefront correction. This represents the knowledge gap that the study attempts to fill by investigating the MLPNN performance for both open and closed AO systems by the zonal correction method. The simulation of the system was accomplished in

MATLAB through assumptions of a static atmosphere and absence of noise for simplification circumstances in order to segregate the performance of prediction for the neural network. The MLPNN consists of three main layers. Each neuron is connected to all neurons in the previous layer, the input, hidden, and output layers. The network input data goes through the input layer, crossing the hidden layer. It is processed by the activation function until received in the output layer [10, 12]. A comparison was made between the closed and open loop of the MLPNN and its counterparts on the traditional method to determine their preference under different turbulence conditions [13, 14].

2. Atmospheric Turbulence Theory

The refractive index affects the light passing through the atmosphere, which arbitrarily changes during time in space, leading to arbitrarily warped propagation [15]. On the other hand, the atmospheric refractive index in constancy is regarded as an indicator of phase distortion of propagated light, which is governed by atmospheric turbulence [16, 17]. Kolmogorov developed the classical theory that is used to interpret turbulence statistically [18]. Kolmogorov's theory applicability range is called the inertial subrange, bounded by an inner scale of turbulence (with a range of millimeters) and an outer scale of turbulence (restricted to a few meters). The inner scale of turbulence is isotropic and statistically has a homogeneous structure. It is unrelated to the outer scale turbulence where the non-isotropic behaviour is prevalent. The effective viscosity and energy dissipated were dominant on a smaller scale than the inner scale of turbulence [19, 20]. In order to explain the statistical turbulence in terms of refractive index, two terms, structure function and power spectral density, were introduced [21]. Since the optical path difference is affected by the variation of refractive index leading to aberration, the difference in refractive index can be described through the averaged square difference, which represents the refractive index structure function [19, 22]

$$D_n(r) = \langle |n(x) - n(x+r)|^2 \rangle = c_n^2 r^{2/3}\,, l_0 \ll r \gg L_0 \quad (1)$$

Where $D_n(r)$ is the refractive index structure-function; l_0 is inner scale turbulence; L_0 is the outer scale turbulence; $n(x)$; $n(x+r)$ is the refractive index in different locations; r is the distance r separated by refractive index in different locations, and c_n^2 is the structure coefficient of refractive index, which indicates the measure of turbulence strength, with the range $\sim(10^{-17} - 10^{-13})m^{2/3}$ for weak to strong turbulence, respectively.

Since the wavefront phase fluctuation is related to the refractive index variation, the phase structure function $D_p(r)$ could be written in terms of the Fried coherence length (r_0) which determines the quality of the atmospheric medium for optical transmission, influenced by the stochastic inhomogeneities present in the refractive index of the atmosphere, as [1, 23].

$$D_p(r) = 6.88\left(\frac{r}{r_0}\right)^{\frac{5}{3}} \quad (2)$$

According to the Kolmogorov model, the refractive index fluctuations arise from atmospheric turbulence described by phase variation to simulate the random behaviour of phase as a phase screen. The power spectral density of the phase fluctuation must be taken into account [24, 25]

$$\Phi_p^K(k) = 0.023 r_0^{-5/3} k^{-11/3} \quad (3)$$

Where $\Phi_p^K(k)$ is Kolmogorov phase power spectral density; and $k = 2\pi/\lambda$ is the wave number.

3. Aim of Study

This work aims to implement a neural network in adaptive optics to predict the atmospheric turbulence that interferes with the telescope image. The performance of computational time is discussed and studied, providing more precision for the DM in reconstructing the wavefront. The feed-forward MLPNN, with a labelled dataset as one of the simplest artificial neural networks, are employed after training using simulated data representing wavefront sensor measurements. The performance was tested using both open and closed-loop adaptive optics systems.

4. Materials and Methodology

In order to employ MLPNN, the Luenberger–Marquardt backpropagation training algorithm was used. The data utilized for the learning were first generated. They were represented by a Kolmogorov phase screen, using a MATLAB simulation program, and grouped into two groups. They were divided according to the training and testing dataset's training ratio. The training data included input and target data, which expressed the wavefront sensor measurements and the smoothed turbulence data, respectively. The connection weights between neurons were adjusted according to the measuring error algorithm, considering the learning rate, batch size, and activation function. The flowchart of the simulation process is shown in Figure 1.

5. The Performance Metrics

The MPLNN performance used the Strehl ratio (SR) as an optical performance metric and average root mean square error (ARMSE) as a statistical one, where the Strehl ratio is calculated as [26]

$$SR = \frac{\max(psf_{perd})}{\max(psf_{ideal})} \quad (4)$$

Where SR = Strehl ratio; $\max(psf_{perd})$ is the maximum value of the predicted wavefront Point Spread Function, and $\max(psf_{ideal})$ is the maximum value of the ideal wavefront Point Spread Function.

The average root mean square error can be represented mathematically as [27]

$$ARMSE = \sqrt{\frac{1}{n}\sum_{i=1}^{n}\left(\phi_{actual} - \phi_{pred}\right)^2} \quad (5)$$

Where ARMSE is the average root mean square error ; n is the total number of elements in the phase screen is ; ϕ_{actual} is the actual (or perturbed) phase screen, and ϕ_{pred} is the predicted phase screen.

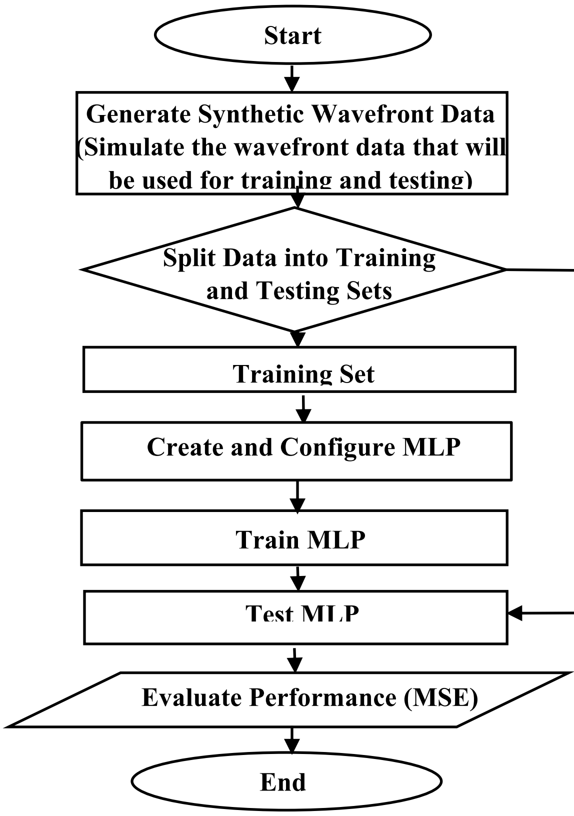

Figure 1: Shows the Blockdiagram of simulation process of MLPNN**.**

6. Computer Simulation Results and Discussion

The MLPNN was implemented to address atmospheric turbulence-induced wavefront distortion in open-loop and closed-loop adaptive optics systems, as illustrated in the following steps:

Step 1: The initial setup for the simulated phase screen includes the following parameters: number of grid points per side $N = 100\, pixels$, Fried coherence length $(r_0 = (0.08 - 0.2)m)$, the outer and inner scale $L_0 = 100m$, $l_0 = 0.01m$ respectively, and wave number $k = 2\pi/\lambda, \lambda = 6.32 \times 10^{-7}\ m.$

Step 2: The induced perturbed wavefront of the atmosphere was generated as a random Gaussian complex matrix vector with unit-variance and zero mean multiplied by the square root of Kolmogorov power spectral density according to Eq.(3). Fast Fourier transform (FFT) algorithm was used to obtain the fundamental component, which was the required output, as in Figure 2.

Step 3: The simulated data (wavefront) was divided using a training ratio of (0.75), resulting in (75%) of the data being used for training and (25%) being used for testing.

Step 4: MLPNN with (50-neuron) hidden layer trained on an Intel(R) Core (TM) i7-13700H CPU with an NVIDIA GeForce RTX 4060 Laptop GPU and its graphic user interface (GUI), illustrated in Figure 3.

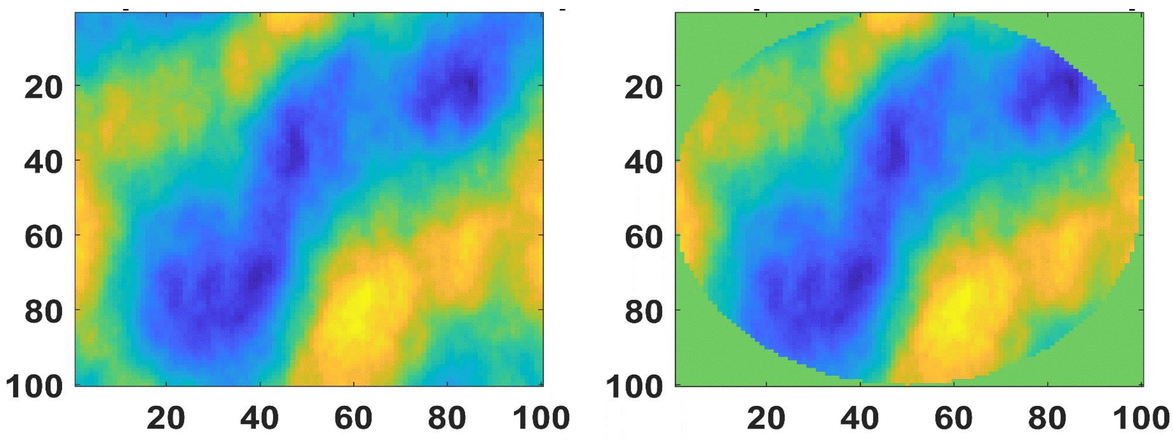

(a) **(b)**

Figure 2: Shows that perturbed phase screen (wavefront) produced by Kolmogorov model (a) without aperture (b) with fit aperture.

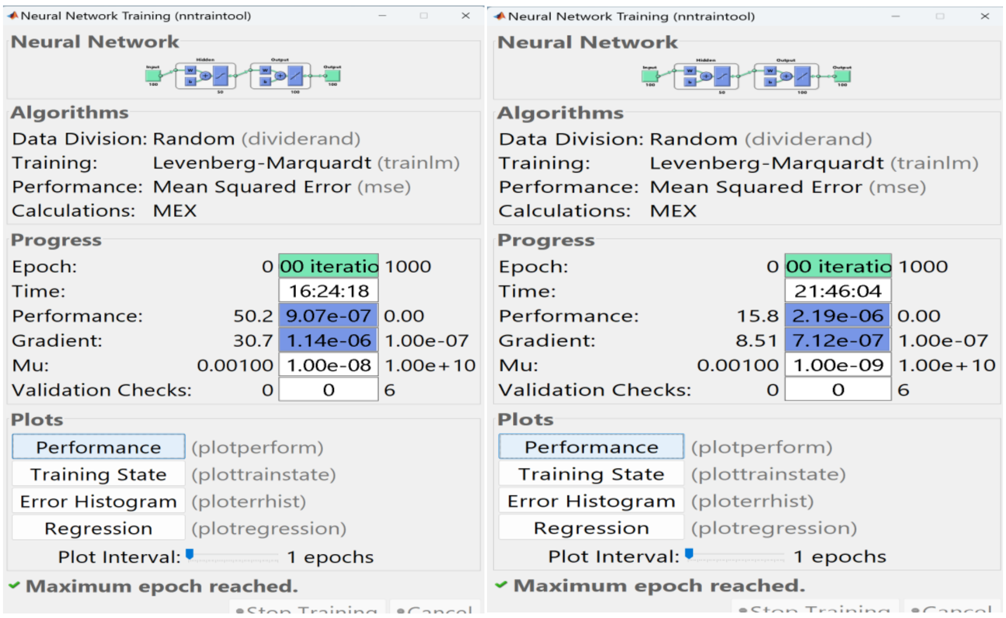

(a) **(b)**

Figure 3: Represents the GUI of MLP neural network with (50-neuron) for both open (a) and closed (a) loop AO systems.

Step 5: The MLPNN architecture that was constructed, trained, and tested provided performance parameters for open and closed-loop AO systems, as well as the corresponding values from the neural network adaptive optics system [11], as shown in Table 1. Additionally, the predicted phase screen with fit aperture using the trained MLPNN was displayed in Figure 4.

Table 1: A comparison between the Contains training, validation, and testing performance parameters for open and closed loop and neural network adaptive optics system work [11].

Parameter	Closed loop	Open loop	AO system [11]
The lowest validation	4.4982×10^{-6}	1.8258×10^{-6}	1.2102×10^{-9}
The gradient	7.1229×10^{-7}	1.1429×10^{-6}	1.026×10^{-5}
The learning rate Mu	1×10^{-8}	1×10^{-9}	1×10^{-9}
The failure of validation (at epoch 1000)	0	0	0
Error histogram interval	$(-0.00509\ to\ 0.005084)$	$(-0.003\ to\ 0.00332)$	$(-3.4\ to\ 3.85)\times10^{-5}$
Error histogram (zero error)	1.3×10^{-6}	1.2×10^{-4}	2.41×10^{-6}
The correlation coefficient(R)	1	1	1

Step 6: The parameters in Table 1 emphasized that the gradient, learning rate Mu, and error histogram (zero error) for the closed loop were generally smaller than those of the open loop. In addition, the comparison with the traditional system simulation showed that it had a preference, despite the difference in the simulated turbulence model. However, the training time and the lowest validation error for the closed loop were slightly more significant than those for the open loop. Compared with [11], it had a preference, despite the difference in the simulation turbulence model.

Step 7: The performance of the MLP neural network for 1000 epochs of training, validation, and testing was obtained through plotting error (Mean squared normalized error) vs. epoch, as shown in Figure 5, where the plot of validation loss decreased to appoint of stability and had a small gap with training loss. Additionally, Figure 6 depicts the network's training state, which displays the gradient, the learning rate (Mu), and the validation failures concerning epochs for open and closed-loop AO systems.

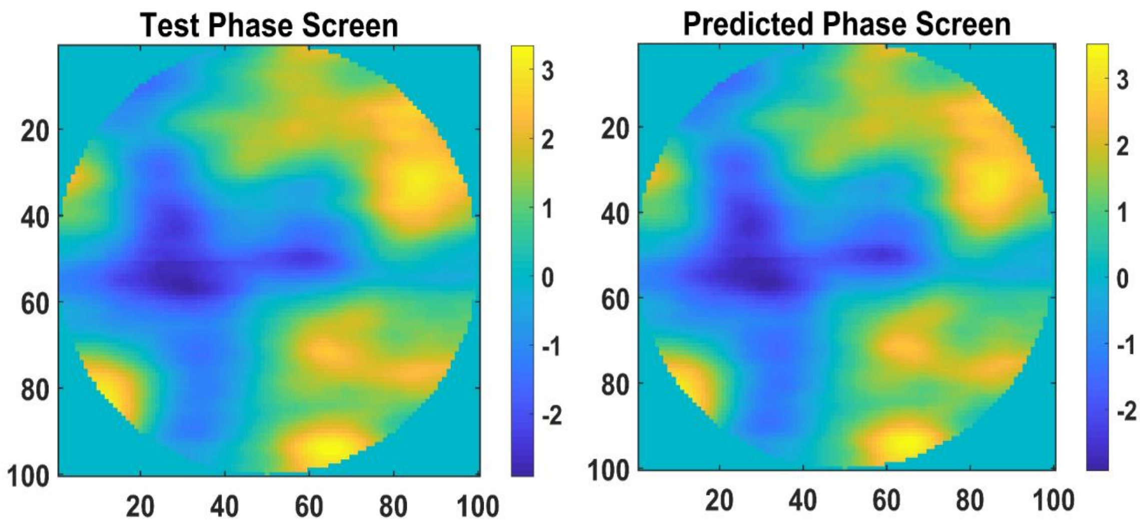

Figure -4 Shows the test phase screen and the predicted phase screen with fit aperture using the trained MLPNN.

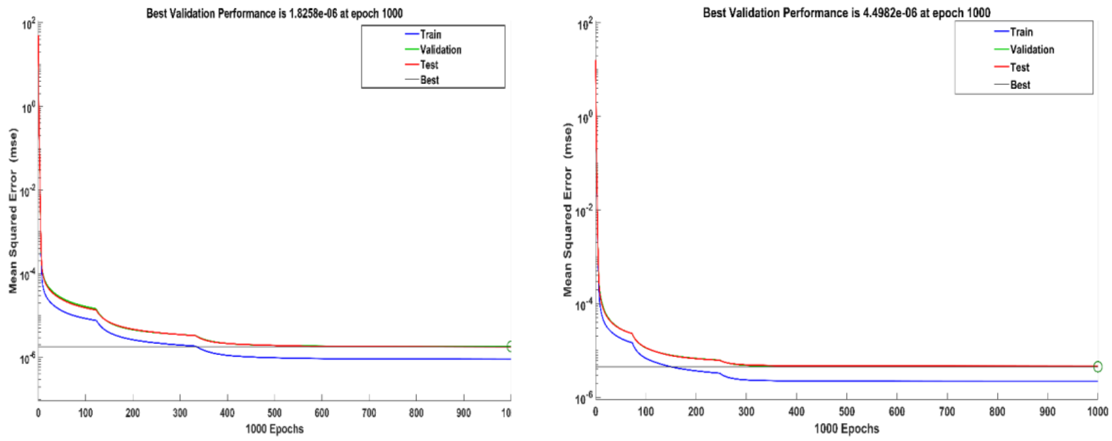

(a) **(b)**

Figure 5: Shows the Performance of MLP neural network for (A) open loop, (B) closed loop AO systems.

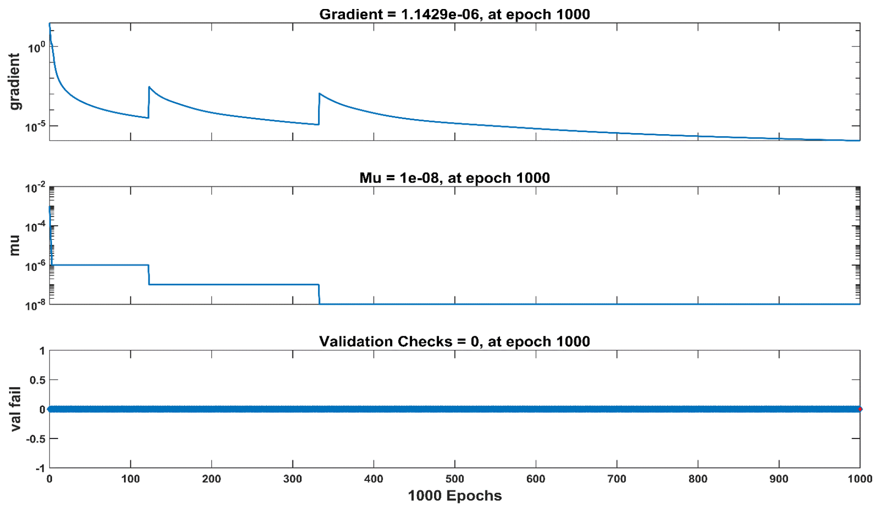

(a)

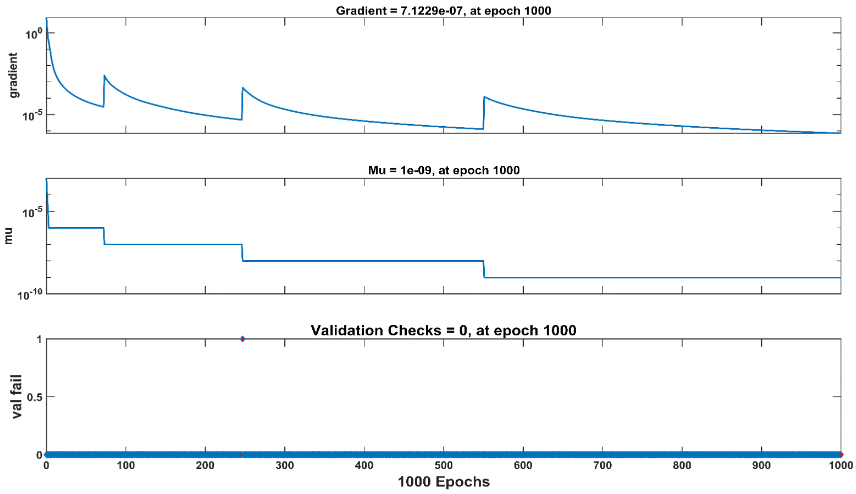

(b)

Figure 6: Represents the gradient, learning rate (Mu), and the failure of validation with respect to epochs for open loop (A) and closed loop (B) AO system.

Where the gradient decreases rapidly at first, indicating fast learning in the early epochs. After that, the curve shows three sudden spikes at approximately epoch 100, epoch 300, and epoch 500. The gradient begins decaying after each spike, showing a continued convergence. This means that the model is converging and learning less dramatically over time. The stepwise decrease in mu suggests the optimizer found the loss surface increasingly suitable for Levenberg-Marquardt updates. The final values of (mu = 1e-08 & mu = 1e-09) indicate the optimizer is in fine-tuning mode, making very small updates with high confidence in curvature estimates. This is a very positive sign for convergence; it shows the optimizer has likely reached or is near a local minimum. The learning rate drops by a factor at specific epochs, resulting in a staircase-like plot. The validation failures plot is entirely a flat line at zero, indicating that no validation failures occurred throughout the 1000 epochs.

Step 8: The error histogram for open and closed loop systems, shown in Figure 7, indicates the presence of outliers in the predicted values. This histogram illustrates the errors between target and predicted values after training a feedforward neural network. The histograms showed a symmetric error distribution in the positive and negative directions around zero, with a bell shape, which refers to the normal distribution. This illustrates that the majority of predictions are near the values of real targets, with a few outlier samples. The similarity distribution of error over datasets, as well as the training, validation, and test curve affinity for both cases, indicates that the model isn't overfit and has a good generalization performance.

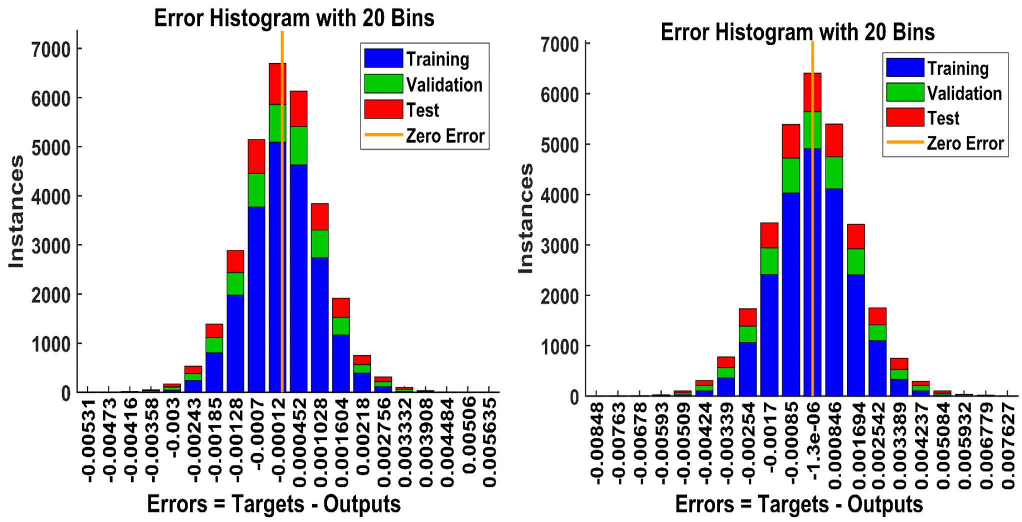

(a   **(b)**

Figure 7: The Error histogram for open loop (A) and closed loop (B) for AO system.

Step 9: The regression plot in Figure 8 exhibits a linear behaviour of the target across the network outputs, which includes training, validation, testing, and all set averages. The variable "*R*" refers to the correlation coefficient between the targets and outputs of the neural network, which is equal to one for all cases.

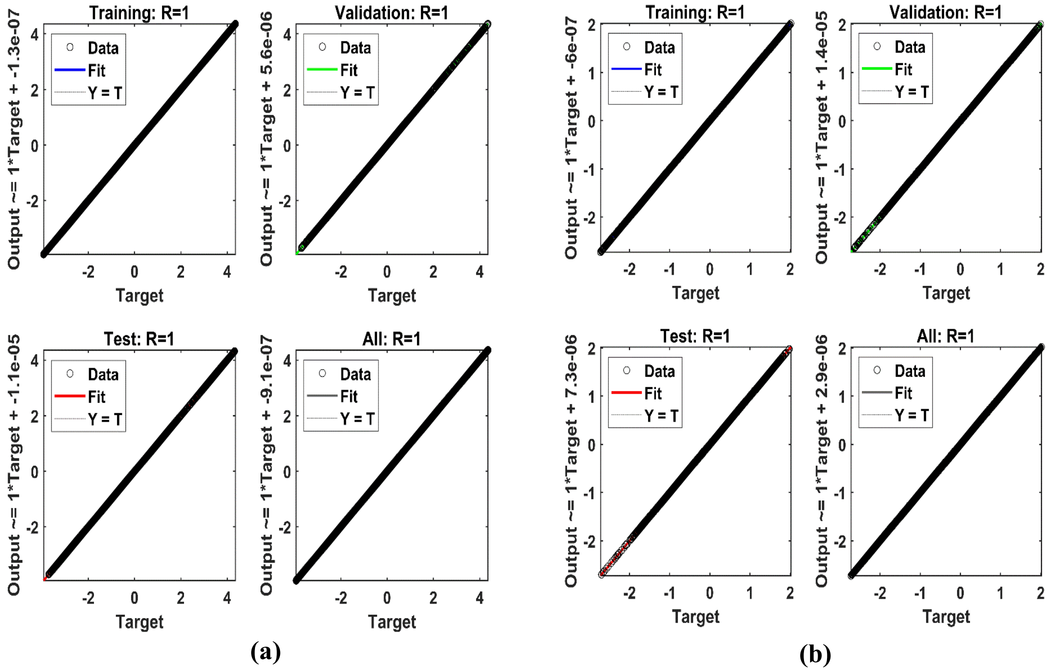

Figure 8: Represents the regression plots, the network outputs with respect to targets for open loop (a) and closed loop (b) AO system.

Step 10: Figure 9 displays the combined graph of target and predicted values for testing the open and closed loop MLPNN after training. Additionally, these Figures show the wavefront RMSE that indicates the positive difference between the target and the predicted value, as determined by the regression model, plotted against the test sample numbers. Clearly shown in Figure 9, the combined graph of the target and the predicted values show a close match for both closed and open systems. However, the RMSE clarified that the closed-loop error is smaller than the open-loop error by an order of(10^{-3}).
Step 11: Equations (4) (5) were used to measure the performed SR and ARMSE of the predicted wavefront from the trained and tested MLPNN and the results were presented in Table 2, where the SR of the closed loop MLPNN value was (0.9132) while that of the open loop was (0.8137). The ARMSE of the closed loop was (0.0028) compared with (0.8952) for the open loop, where the difference was noticeable between the two cases.
Step 12: After running the main program and completing the training state, the trained program was used as an external function to predict the phase screen (wavefront) for any new perturbed wavefront in a few seconds. Table 3 presents the results of the comparison between the saved results from the main program and the results from the external function program for both open and closed-loop systems. The results showed that the external function program demonstrated a (0.9030) SR of the closed loop against (0.7588) for the open loop. Additionally, ARMSE for the closed loop value was equal to (0.10211), whereas its value for the open loop was (0.9523). Furthermore, the main program presented a (0.9132) SR for the closed loop, while that of the open loop was (0.8137). The ARMSE of the closed loop was (0.0028) compared with (0.8952) for the open loop.
Moreover, the target and the predicted value combined curves and RMSE are plotted in Figure 10. As noticed in Figure 10, RMSE for the closed loop is smaller, and the test target complements the predicted output more than that of the open loop.

Table 2: Contains the SR and ARMSE of predicted wavefront from the trained and tested MLP neural network.

AO System type	ARMSE	SR of the compensation process
Open loop	0.8952	0.8137
Closed loop	0.0028	0.9132

Table 3: Contains the SR and ARMSE for the wavefront predicted.

Performance parameters	MLPNN from external function phase prediction		MPLNN main program phase prediction	
	Open loop AO System	Closed loop AO System	Open loop AO System	Closed loop AO System
SR	0.7588	0.9030	0.8137	0.9132
ARMSE	0.9523	0.10211	0.8952	0.0028

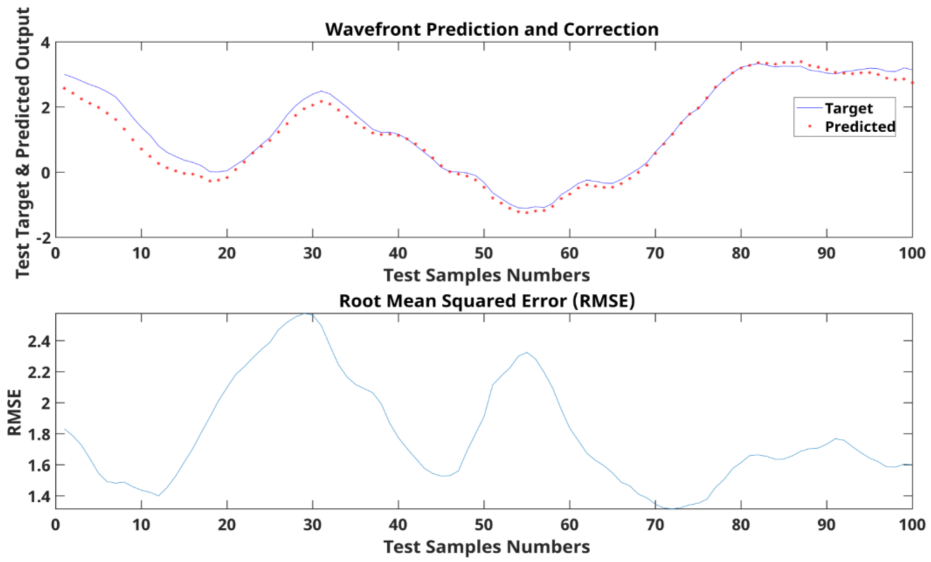

(a)

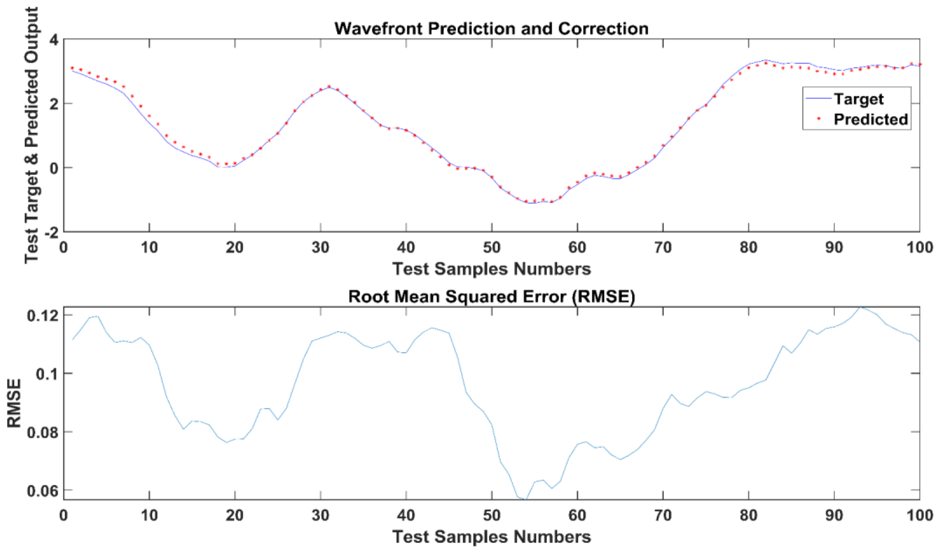

(b)

Figure 10: Illustrates the combined graph of target and predicted values, as well as RMSE for the open loop(a) and closed loop (b) testing MLPNN with saved phase screen test.

Step 13: The phase screen of different turbulence strength was used to test the trained network by adopting the Fried coherence length (r_0) as indictor. The values of SR and ARMSE, which were presented in Table 4 exhibited an increase in SR at $(\mathrm{r}_0 = 0.08m)$ from (0.1467) in open loop to (0.4328) for closed loop, with ARMSE decreasing from (1.3732) for the open loop to (0.9394) for the closed loop. This indicated that the closed-loop system effectively reduced wavefront errors, leading to improved optical quality even under strong turbulence. On the other hand, at $(\mathrm{r}_0 = 0.20m)$ the rise in SR for the closed loop was (0.9283) compared with its value (0.8414) for the open loop. The ARMSE dropped to (0.2857) for the closed loop compared to that of the open loop (0.4411). These results confirmed that the closed-loop system became increasingly effective in moderate to weak turbulence conditions, aligning with physical expectations where higher r_0 corresponded to better atmospheric conditions. While the result of the traditional method simulation showed an increase in SR at $(\mathrm{r}_0 = 0.10m)$ from (0) in open loop to (0.39) for closed loop, with the ARMSE decreasing from (721) for the open loop to (189) for the closed loop. Whereas the trained network reached an SR of 0.5398 and reduced ARMSE to 0.8425. Furthermore at $(\mathrm{r}_0 = 0.20m)$ the rise in SR for the closed loop was (0.86) compared with its value (0.06) for the open loop. The ARMSE dropped to (76) for the closed loop compared to that of the open loop (151)[13]. Although the proposed method attained an SR of 0.9283 and ARMSE of 0.2857, indicating a more accurate phase reconstruction. Moreover, the proposed network showed superior performance, particularly in stronger turbulence. Additionally, the relationship between SR and ARMSE versus the Fried parameters, shown in Figures 11 and 12, supports these findings, showing a clear inverse relationship between SR and ARMSE as a function of r_0. As r_0 increased (turbulence weakens), SR improved, and ARMSE decreased, validating the efficacy of the trained network in closed-loop correction across a range of atmospheric conditions.

Table 4: Contains the SR and ARMSE for different Fried coherence lengths (r_o) tested in closed and open loop AO systems.

r_0(m)	SR		ARMSE	
	Closed loop	Open loop	Closed loop	Open loop
0.8	0.4328	0.1467	0.9394	1.3732
0.10	0.5398	0.3288	0.8425	1.1656
0.12	0.7658	0.5883	0.5223	0.7382
0.14	0.8525	0.6916	0.4058	0.6202
0.16	0.8664	0.7273	0.4375	0.6113
0.18	0.9028	0.7984	0.3150	0.4707
0.20	0.9283	0.8414	0.2857	0.4411

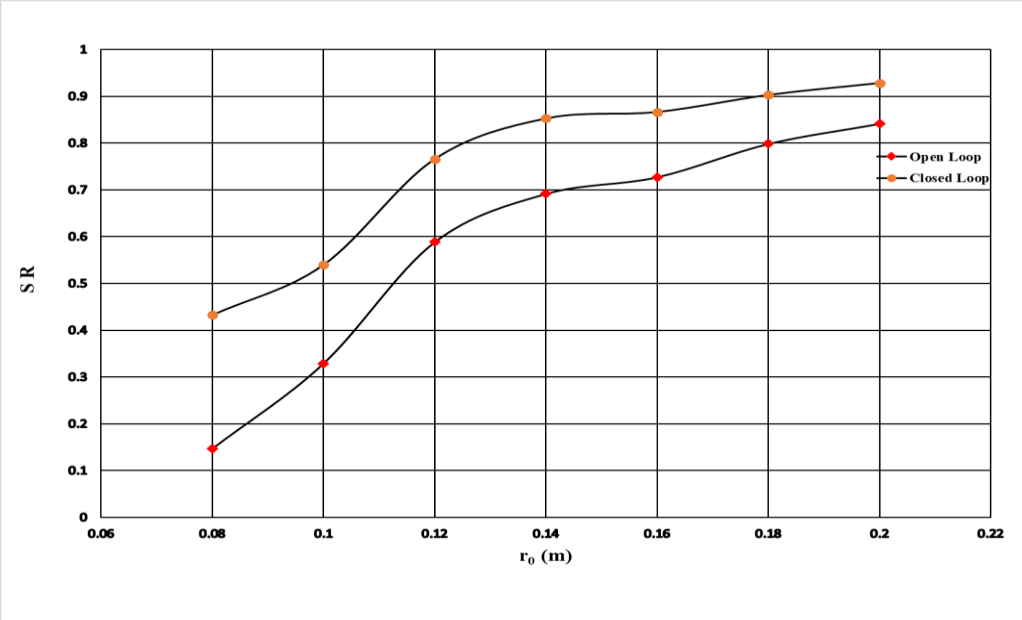

Figure 11 : Illustrates the relation between SR and r_0 for open and closed loop AO system.

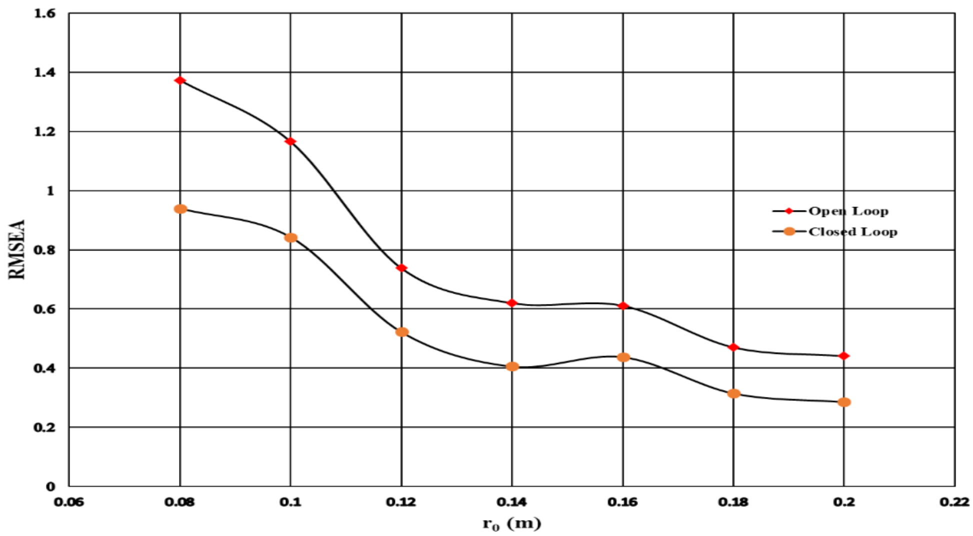

Figure 12: Illustrates the relation between ARMSE and r_0 for open and closed loop AO system.

According to the Kolmogorov theory, the assumptions of the static behaviour of the atmosphere lead to isotropic and homogenous mediums. Moreover, neglecting noise is associated with the turbulent wavefront. These assumptions limit the present work.

7. Conclusion

An MLPNN was utilized in adaptive optics to predict the distorted wavefront affected by atmospheric turbulence and to reconstruct a compensated wavefront. The network was trained and tested to develop an accurate wavefront sensor model. Based on the training and testing performance of MLPNN, the closed-loop system demonstrated the best performance parameters compared to the open-loop system. Moreover, the correlation coefficient, which was equal to one, indicated a perfect correlation or, in other words, an exact linear relationship between outputs and targets. The lower RMSE and the closer match between the target and the predicted values of closed-loop MLPNN made it preferable to an open loop.

The external function program demonstrates an approximate value of SR and ARMSE comparison with the main program. However, the time it takes for prediction is minimal and cannot be compared with the long duration of the main program. Across varying levels of turbulence, it was demonstrated that the relationship between SR and ARMSE versus r_0 shows that as r_0 increases, SR tends to increase while ARMSE decreases in both open- and closed-loop systems. This is attributed to the increase in prediction efficiency as the turbulence strength decreases. Due to the limitations of static atmosphere behaviour, the lack of wavefront sensor noise, as well as the rarity of closed-loop AO research, these could affect the training model. It is recommended that further research should choose the closed loop in the case of high turbulence instead of the open loop. Additionally, include an alternative turbulence model alongside the Kolmogorov model. Also, apply the external function method to the trained closed-loop MLPNN model. As a result, the closed-loop system performed better under stronger turbulence compared to the open-loop system, thanks to its favorable performance at higher turbulence levels. Overall, the testing phase demonstrated that the trained closed-loop MLPNN approach holds strong potential for adaptive optics applications, effectively addressing the shortcomings of wavefront prediction.

8. Acknowledgements

The authors wish to express their heartfelt gratitude to the editors and anonymous reviewers for their thoughtful feedback, constructive suggestions, and invaluable insights, which have greatly enriched and elevated the quality of this paper.

References

[1] F. Roddier, *Adaptive Optics in Astronomy*. Cambridge,United Kingdom: Cambridge University Press, 1999, p. 407.

[2] J. M. Beckers, "Adaptive Optics for Astronomy: Principles, Performance, and Applications," *Annual Review of Astronomy and Astrophysics,* vol. 31, pp. 13-62, 1993.

[3] M. van Kooten, N. Doelman, and M. Kenworthy, "Impact of Time-Variant Turbulence Behavior on Prediction for Adaptive Optics Systems," *J. Opt. Soc. Am. A,* vol. 36, no. 5, pp. 731-740, 2019.

[4] Y. Guo *et al.*, "Adaptive Optics Based on Machine Learning: A Review," *OEA,* vol. 5, no. 7, pp. 200082-1-200082-20, 2022.

[5] C. Li, M. Xia, Q. Mu, B. Jiang, L. Xuan, and Z. Cao, "High-Precision Open-Loop Adaptive Optics System Based on LC-SLM," *Opt. Express,* vol. 17, no. 13, pp. 10774-10781, 2009.

[6] J. W. Hardy, *Adaptive Optics for Astronomical Telescopes*. NY,USA: Oxford University Press, 1998, p. 448

[7] A. P. Wong *et al.*, "Predictive Control for Adaptive Optics Using Neural Networks," *Journal of Astronomical Telescopes, Instruments, and Systems,* vol. 7, no. 1, pp. 019001-0190022, 2021.

[8] J. Osborn *et al.*, "Using Artificial Neural Networks for Open-Loop Tomography," *Opt. Express,* vol. 20, no. 3, pp. 2420-2434, 2012.

[9] J. Osborn *et al.*, "Open-loop tomography with artificial neural networks on CANARY: on-sky results," *MNRAS,* vol. 441, no. 3, pp. 2508-2514, 2014.

[10] C. González-Gutiérrez *et al.*, "Comparative Study of Neural Network Frameworks for the Next Generation of Adaptive Optics Systems," *J. Sens,* vol. 17, no. 6, pp. 1-14, 2017.

[11] R. N. Hassan, "Compensation of Atmospheric Turbulence Phase Distortion Using Neural Network Adaptive Optics," *Iraqi j. phys.,* vol. 22, no. 1, pp. 53-74, 2024.

[12] F. García Riesgo, S. L. Suárez Gómez, J. D. Santos, E. Díez Alonso, and F. Sánchez Lasheras, "Overview and Choice of Artificial Intelligence Approaches for Night-Time Adaptive Optics Reconstruction," *Mathematics,* vol. 9, no. 11, p. 1220, 2021.

[13] M. K. Mirdan, R. N. Hassan, and B. Q. Al-Aboodi, "MODELING AND COMPARISON OF CLOSED-LOOP AND OPEN-LOOP ADAPTIVE OPTICS SYSTEMS," *Euro. Sch. J,* vol. 3, no. 5, pp. 16-25, 2022.
[14] M. K. Mirdan, R. N. Hassan, and B. Q. Al-Aboodi, "Performance Simulation for Adaptive Optics Technique Using OOMAO Toolbox," *Karbala Int. J. Modern Sci.,* vol. 8, no. 3, pp. 306-312, 2022.
[15] J. D. Schmidt, *Numerical Simulation of Optical Wave Propagation with Examples in MATLAB*. Washington , USA: Society of Photo-Optical Instrumentation Engineers (SPIE) Press, 2010, p. 212.
[16] K. Wang *et al.*, "Generation of Non-Kolmogorov Atmospheric Turbulence Phase Screen Using Intrinsic Embedding Fractional Brownian Motion Method," *Optik,* vol. 207, p. 164444, 2020.
[17] T. Helin, S. Kindermann, J. Lehtonen, and R. Ramlau, "Atmospheric Turbulence Profiling With Unknown Power Spectral Density," *Inverse Problems,* vol. 34, no. 4, pp. 1-32, 2018.
[18] A. N. Kolmogorov, "Dissipation of energy in the locally isotropic turbulence," in *Dokl. Akad. Nauk. SSSR*, 1941, vol. 32, pp. 19-21.
[19] L. C. Andrews, *Field Guide to Atmospheric Optics* (SPIE Field Guides). Washingtion, USA: SPIE-The International Society for Optical Engineering, 2019.
[20] I. Toselli, "Introducing the Concept of Anisotropy at Different Scales for Modeling Optical Turbulence," *J. Opt. Soc. Am. A,* vol. 31, no. 8, pp. 1868-1875, 2014.
[21] L. C. Andrews and R. L. Phillips, *Laser Beam Propagation Through Random Media*, 2nd ed. Washingtion, USA: SPIE Optical Engineering Press, 2005.
[22] H. S. Ali, "Performance Estimation of Solar Imagery Using Different Types of Atmospheric Turbulence Models," *Iraqi Journal of Science,* pp. 4579-4590, 2023.
[23] D. L. Fried, "Statistics of a Geometric Representation of Wavefront Distortion," *Journal of the Optical Society of America* vol. 55, no. 11, pp. 1427-1435, 1965.
[24] R. J. Noll, "Zernike Polynomials and Atmospheric Turbulence," *J. Opt. Soc. Am.,* vol. 66, no. 3, pp. 207-211, 1976.
[25] S. K. Saha, *Aperture Synthesis: Methods and Applications to Optical Astronomy*. NY , USA: Springer 2010, p. 466.
[26] D. Wegner, "Imaging simulation of atmospheric turbulence based on phase screen methods," Ph.D. thesis, Karlsruher Institut für Technologie (KIT), Karlsruhe ,Germany, 2022.
[27] A. Kharwal, *Machine Learning Algorithms: Handbook*. Bangalore,India: Clever Fox Publishing, 2023, p. 234.